

Condensation of cloud microdroplets in homogeneous isotropic turbulence

Alessandra S. Lanotte

CNR - Istituto di Scienze dell'Atmosfera e del Clima,
Via Fosso del Cavaliere 100, I-00133 Roma, Italy
and INFN, Sezione di Lecce, I-73100 Lecce, Italy

Agnese Seminara*

Harvard University, School of Engineering and Applied Sciences,
29 Oxford Street, 02138, Cambridge - MA, USA

Federico Toschi

CNR - Istituto per le Applicazioni del Calcolo, I-00185 Roma, Italy
INFN, Sezione di Ferrara, Ferrara, Italy

* *Corresponding author address:* Agnese Seminara Harvard University, School of Engineering and Applied Sciences, 29 Oxford Street, 02138, Cambridge - MA, USA.
E-mail: seminara@seas.harvard.edu

Abstract

The growth by condensation of small water droplets in a three-dimensional homogeneous isotropic turbulent flow is considered. Within a simple model of advection and condensation, the dynamics and growth of millions of droplets are integrated. A droplet-size spectra broadening is obtained and it is shown to increase with the Reynolds number of turbulence, by means of two series of direct numerical simulations at increasing resolution. This is a key point towards a proper evaluation of the effects of turbulence for condensation in warm clouds, where the Reynolds numbers typically achieve huge values. The obtained droplet-size spectra broadening as a function of the Reynolds number is shown to be consistent with dimensional arguments. A generalization of this expectation to Reynolds numbers not accessible by DNS is proposed, yielding upper and lower bounds to the actual size-spectra broadening. A further DNS matching the large scales of the system suggests consistency of the picture drawn, while additional effort is needed to evaluate the impact of this effect for condensation in more realistic cloud conditions.

1. Introduction

The growth of microdroplets by condensation is a long-standing problem of cloud physics (Pruppacher and Klett (1997)), meteorology (see e.g. IPCC-WGI (2001)), medicine (Martonen (2000)) and engineering (Zhao et al. (1999)). A fundamental understanding of key issues such as the turbulent mixing inside clouds, or the interaction of turbulence with microphysics is important for a variety of applications (the parameterization of small scales in large scales models, the analysis of radiative transfer through clouds, the accurate prediction of the initiation of precipitation). The peculiar features of turbulence, influencing the motion on a wide range of space-time scales, can alter significantly the condensation process, providing a strongly fluctuating and intermittent moist environment. This is a well-known concept in engineering, where turbulence is considered as a key ingredient for the optimization of fuel-air mixing and of the rate of fuel vaporization in engines (Zhao et al. (1999)). Similar ideas have a long history in cloud physics: turbulence plays a role both in collision processes (Saffman and Turner (1956); Shaw (2003); Sundaram and Collins (1997); Ghosh et al. (2005); Falkovich et al. (2002); Wang et al. (2006); Wilkinson et al. (2006)) and in condensation. In this work we will focus particularly on the latter process.

Condensation is a fundamental process for the early stages of cloud evolution. It is the only mechanism providing a growth of cloud droplets immediately after their formation, when they are few micrometers in size. The initiation of collisions and coalescence occurs when a few droplets become large enough to fall - a radius of $20\text{ }\mu\text{m}$ is commonly considered as a threshold. For these droplets, collisions are much more efficient than condensation as a growth mechanism. Indeed, after nucleation, droplet radius grows roughly one order of magnitude by condensation. In a timescale comparable to that of condensation, collisions produce raindrops, bridging a gap of about two orders of magnitude in size. However, the high efficiency of the latter is strongly influenced by the general features of the former. In particular, gravitational collisions are highly effective when the previous condensation process produces a population of droplets spanning a large variety of sizes. Uniform condensational growth leads to narrow droplet-size spectra instead (see e.g. Squires (1952); Lee and Pruppacher (1977)). Indeed, provided that all droplets grow in similar ambient conditions, small droplets grow faster than large ones and thus all droplets finally tend to converge to the same size. This yields the long-standing problem of the bottleneck between condensation and collision-coalescence.

The presence of broad droplet-size distributions has been detected via *in situ* measurements in warm clouds under very different conditions, Warner (1969). Still, this observation eludes full theoretical understanding despite the number of different approaches developed to this purpose. Some of them rely on the effects of entrainment and mixing with non-cloudy air occurring in the regions of the cloud near the boundaries (see, e.g., Blyth (1993)). However, broad spectra are also observed inside the inner adiabatic cores, as reported by Brenguier and Chaumat (2001), where no boundary effects can possibly explain their presence. Droplets themselves have been proposed to be sources of local variability in the environmental conditions. Indeed, droplet evaporation is an internal source of turbulent kinetic energy due to cooling associated to the absorption of latent heat, coupled with buoyancy (see Andrejczuk et al. (2004); Malinowski et al. (1998); Korczyk et al. (2006)). Moreover, the presence of droplets locally changes the water vapor content through phase change, Shaw et al. (1998). The general conclusion is that these microscopic fluctuations influence the process of mixing occurring at the interface between cloud and clear-air. Also, the presence of ultra-giant condensation nuclei has been proposed to explain the large raindrops production (Johnson (1982)). Other properties such as

salinity and surface curvature may produce absolute and relative broadening, as proposed in Korolev (1995).

Stochastic fluctuations of the environmental conditions, induced by turbulence have been suggested as a broadening mechanism since the '60s when the theory of stochastic condensation was first proposed, see e.g. Mazin (1968); Levin and Sedunov (1966); Bartlett and Jonas (1972). This approach explains droplet spectra broadening by observing that fluctuations of the ambient conditions make droplets grow at different rates. This simple idea is very powerful in that it concerns the whole cloud, regardless of the presence of additional microscopic mechanisms, the influence of ultra-giant nuclei and/or boundary effects such as mixing with dry air and entrainment. Although all these ingredients play a role in the huge natural laboratories represented by clouds, their contribution may vary according to different conditions. On the contrary, turbulence is a very good candidate as general broadening mechanism within convective warm clouds. At a Reynolds number approaching $Re \sim 10^8$, turbulence is known to be highly intermittent, with statistics strongly deviating from a Gaussian one and a substantial probability of fluctuations far exceeding the standard deviation (see, e.g., Frisch (1995)). This means that droplets coming close one to the other might have previously experienced disparate conditions, thus invalidating any expectation based on uniform condensation. Here we show that some qualitative features emerging from a simple idealized setting may be well present in more complex models, just because they are consequences of basic properties of turbulence itself. In view of this purpose, under consistent hypothesis, we consider a simple but rather general model for condensation to be detailed below.

Droplet growth in a fully developed turbulent flow can not be treated analytically and the numerical analysis becomes a fundamental tool of investigation. Numerical simulations of cloud turbulence are very demanding because of the huge number of active degrees of freedom (the microscale Reynolds number varies as a function of the spatial resolution approximately as $Re_\lambda \sim N^{2/3}$). As a consequence of the spatial structure of the turbulent fields, direct numerical simulations (DNS) can either focus on large-scale structures as done by Celani et al. (2005, 2007), or resolve the small scale features as in Vaillancourt et al. (2001, 2002); Korolev and Mazin (2003); Andrejczuk et al. (2004). The two choices are actually mutually exclusive due to finite computing resources and both have strong and weak points (see Section 2, for further details). Here we will try to take advantage of both these approaches, to achieve a deeper understanding on the role of turbulent fluctuations for the problem at hand.

In a nutshell, we first evaluate the spreading of droplet-size distribution through a series of direct numerical simulations, at increasing resolution, matching the small scale features. Not surprisingly, each single DNS gives a small degree of spreading, as already pointed out in previous works focusing on small rising fluid parcels (see e.g. Vaillancourt et al. (2002); Korolev and Mazin (2003); Andrejczuk et al. (2004)). However this only tells us that turbulence at the smallest scales alone fails to explain the fast broadening of droplet-size distributions observed in clouds. Then, we evaluate the dependence of the size spectra broadening on the turbulent Reynolds number, i.e. on the range of spatial scales resolved. The broadening is found to increase with the Reynolds number of turbulence.

Since the Reynolds numbers of real cloud turbulence are several orders of magnitude larger than those described by DNS, this increase must be accounted for when assessing the role of turbulence for condensation in clouds. In order to get more insight on this point, we analyze the trend of the size-spectra broadening as a function of the Reynolds number. It is quite natural

to derive, on the basis of consistent assumptions, expectations for the observed broadening at large Reynolds number. Within the model adopted, we derive upper and lower bounds on the trend through a dimensional analysis of the system equations. The upper bound is obtained by neglecting the vapor depletion due to condensation onto cloud droplets. We argue that this should be significant at small time lags and small Reynolds numbers, and we show that this is consistent with two series of DNS performed. We then reason that the lower bound, where the vapor fluctuations are considered immediately depleted for condensation/evaporation, should be more significant at high Reynolds numbers and large time lags. A further DNS matching the large scales of the problem suggests consistency with the argument.

The paper is organized as follows. In Section 2 we introduce the model for the time evolution of the vapor field and the droplets advected by the turbulent air flow. Section 3 is devoted to the numerical approach and DNS details. Results concerning the spreading of droplet-size spectrum are discussed in Section 4, while in Section 5 conclusions and perspectives will follow.

2. Model equations and numerical procedures

We focus on a turbulent velocity field advecting vapor and droplets. The latter undergo size changes for evaporation or condensation of the surrounding vapor. The three-dimensional velocity field \mathbf{v} evolves according to the Navier-Stokes equations for an incompressible flow,

$$\partial_t \mathbf{v} + \mathbf{v} \cdot \nabla \mathbf{v} = -\frac{\nabla p}{\rho_a} + \nu \Delta \mathbf{v} + \mathbf{f}, \quad \nabla \cdot \mathbf{v} = 0, \quad (1)$$

where p is the pressure, ρ_a is the air density and \mathbf{f} is an external statistically homogeneous and isotropic forcing, providing a turbulent stationary flow. In eq.1, $\nu \approx 0.15 \text{ cm}^2/\text{s}$ is the air kinematic viscosity. Note that turbulence in clouds is generated by large-scale turbulent fluctuations which can be strongly anisotropic. Indeed the presence of gravity - here neglected - introduces a preferential direction through large-scale thermal gradients and buoyancy, the engine of convective motions. However, we can assume that for sufficiently small internal cloud cores, vertical stratification of the environment can be neglected and the small-scale flow is essentially forced by nonlinear transfer from larger scales, rather than by buoyancy. Isotropy can thus be assumed for these scales of motion. In Vaillancourt and Yau (2000), the authors argue that this should be valid in warm-cloud cores for spatial scales up to $L \sim 100 \text{ m}$. In addition to large-scale thermal gradients, anisotropy is also produced through buoyancy by microscopic temperature fluctuations. Sedimenting droplets can evaporate, absorbing latent heat and thus locally cooling the environment. There are conditions for which this effect can be important for the cloud-clear air mixing at small turbulent kinetic energy rates (Korczyk et al. (2006); Malinowski et al. (1998); Andrejczuk et al. (2004)). However, provided that we focus on the inner adiabatic core, away from the cloud boundaries, we can neglect this microscopic source of anisotropic fluctuations as a first approximation. With equation (1), we focus on the turbulent motion of in-cloud air, neglecting the role of convective motions. Note that previous two-dimensional DNS (Celani et al. (2005, 2007)), suggest that the qualitative effects of turbulence on condensation do not rely specifically on the statistical details of the turbulent regime analyzed.

Water vapor molecules carried by the turbulent velocity field are the source for droplet growth by condensation. The relevant quantity for droplet condensation/evaporation is the supersaturation, which quantifies the presence of vapor available for cloud particles growth. Supersaturation is defined as $s := e/e_s - 1$, where e and e_s are the vapor pressure and the saturation

vapor pressure respectively. Droplets are able to grow when the surrounding vapor content exceeds the saturation point (s positive in equation (4), moist air). On the contrary droplets tend to evaporate when s is negative (dry regions). Exhaustive *in situ* measures of the small-scale statistics of the vapor field are not available so far. Therefore, different models proposed cannot yet be validated by direct comparison with real data.

For the sake of generality, we adopt here the simplest generalization of the well-known model proposed in Twomey (1959). While Twomey considered a one-dimensional equation for the time-dependent supersaturation function, here we consider the turbulent vapor to fluctuate both in space and time. For this reason we introduce the supersaturation as a field $s(\mathbf{x}, t) := \frac{e}{e_s}(\mathbf{x}, t) - 1$, that quantifies the amount of vapor which is present at point \mathbf{x} at time t . Since $s(\mathbf{x}, t)$ is allowed to fluctuate from positive to negative values, dry and moist regions can coexist at the same time.

The generalization of Twomey's equation (see also Pruppacher and Klett (1997); Shaw (2003); Korolev and Mazin (2003)), for the supersaturation field is an advection-diffusion equation:

$$\partial_t s + \mathbf{v} \cdot \nabla s = \kappa \Delta s + A_1 w - \frac{s}{\tau_s}. \quad (2)$$

Here we assume that the scalar field $s(\mathbf{x}, t)$ is passively advected by the turbulent flow $\mathbf{v}(\mathbf{x}, t)$ which is not affected by its presence. In this way, we are neglecting the compositional effects of vapor on the buoyancy forces acting on the flow, that are generally thought to be small (see Stevens (2005)). In equation (2), $\kappa \approx 10^{-5} \text{m}^2 \text{s}^{-1}$ is the molecular diffusivity of water vapor in air and $w(\mathbf{x}, t)$ is the vertical component of the turbulent velocity field \mathbf{v} .

The term $A_1 w$ acts as a source/sink term of supersaturation resulting from the variation in temperature and pressure with height. It can be computed by assuming that (i) air pressure is quasi-hydrostatic, (ii) the pressure of dry air is similar to that of moist air, (iii) the motion inside the cloud core is adiabatic (temperature changes with vertical motion according to a dry adiabatic lapse rate and with latent heat effects as described below) and (iv) the atmosphere is not far from saturation. These standard arguments (see e.g. Pruppacher and Klett (1997); Korolev and Mazin (2003)) yield

$$A_1 = \frac{Lg}{R_v c_p T^2} - \frac{g}{R_a T}$$

where L is the latent heat of evaporation, R_v and R_a are the gas constants for vapor and dry air, c_p is the specific heat at constant pressure, and g is the gravitational acceleration. A_1 can be interpreted as a global supersaturation gradient.

The term $-s/\tau_s$ accounts for the double effect of condensation/evaporation on supersaturation: on one side the phase change directly modifies the water vapor content, on the other side it locally modifies temperature due to absorption or release of latent heat. In dry regions, $s(\mathbf{x}, t) < 0$, droplets tend to evaporate releasing vapor and cooling the environment; here, the term $-s/\tau_s$ is a source of supersaturation. Conversely in moist regions droplets tend to absorb vapor for condensation and to release latent heat, and $-s/\tau_s$ acts as a sink term. The parameter τ_s is the relaxation timescale of the supersaturation and depends locally on the concentration and size of droplets. In each elementary volume V , τ_s is defined as (see appendix A):

$$\tau_s^{-1} = \frac{4\pi\rho_w A_2 A_3}{V} \sum_{i=1}^n R_i, \quad (3)$$

where R_i are the radii of the n droplets inside the considered volume; A_2 is a function of thermodynamic parameters (see appendix A); ρ_w is the water density; A_3 is the rate of droplet radius growth by condensation (see equation (4)). In the numerical procedure, we consider each droplet to affect the value of τ_s in the eight nodes of the grid cell surrounding its position. The weight of the contribution to each node is calculated via a three-linear extrapolation. Table 1 shows the reference values of these parameters used in the numerical experiments.

Note that Twomey’s one-dimensional equation for s is derived under a given temperature profile, neglecting fluctuations. It is difficult to quantify temperature fluctuations in clouds, since *in situ* microscale cloud data are unavailable. For what concerns the vapor field, this amounts to neglect an additional source of fluctuations induced by temperature advection and diffusion. The remarkable feature of the simple model identified by equations (1) and (2) is that, despite its simplicity, it allows to identify nontrivial mechanisms leading to the spreading of the size spectra.

Given the evolution equation for the Eulerian turbulent fields, we can now introduce the Lagrangian dynamics of cloud particles and the time evolution of their radii. A complete description of the relation between the water vapor and the size of a droplet would imply an integral equation for the local dynamics occurring at the droplet surface. Note that, however, the typical timescales associated with the diffusional growth of an isolated droplet are much smaller than the fastest timescale associated with turbulent changes in the ambient conditions Pruppacher and Klett (1997). Therefore we can consider the droplet to be instantaneously in equilibrium with the surrounding vapor (a detailed quantification of this assumption is given, e.g., in Vaillancourt et al. (2001), where the authors argue that it should be valid in the condensation stage, for kinetic energy dissipation rates of about $\epsilon \approx 10^{-3} m^2 s^{-3}$ that we consider here). Under basic assumptions¹ we end up with the following equation for the i -th droplet growth rate (see also Pruppacher and Klett (1997) for further details),

$$\frac{dR_i(t)}{dt} = A_3 \frac{s(\mathbf{X}_i(t), t)}{R_i(t)}. \quad (4)$$

Here A_3 is a function of the local conditions, air temperature and pressure, and assumed to be constant throughout the entire volume (variations of this parameter with temperature in typical warm cloud conditions are smaller than 3%). According to equation (4), the growth rate varies from a droplet to another, since it depends on the supersaturation fluctuation $s(\mathbf{X}_i(t), t)$ measured along the trajectory $\mathbf{X}_i(t)$ of the single droplet. Due to turbulent transport, initially close droplets separate very rapidly and eventually experience disparate values of supersaturation throughout the entire cloud volume. This is the most important difference with respect to Twomey’s model where all the droplets are exposed to the same supersaturation value.

Cloud droplets can be described as independent, Stokes particles, whose trajectories $\mathbf{X}_i(t)$ and velocities $\mathbf{V}_i(t)$ evolve according to:

$$\frac{d\mathbf{X}_i(t)}{dt} = \mathbf{V}_i(t) \quad (5)$$

¹(i) Droplets are considered spherical (significant deformations from the spherical shape are typical of much larger drops, from sizes of hundreds of μm); (ii) the coefficient A_3 is not significantly altered by either the chemical composition of droplets or the size of the droplet itself (this holds for droplets already activated onto condensation nuclei); (iii) curvature and salinity corrections to the supersaturation at droplet surface (described by classical Köhler theory) are neglected for simplicity - these are generally thought to be small for radii larger than few microns (see e.g. Korolev and Mazin (2003); Pruppacher and Klett (1997)).

$$\frac{d\mathbf{V}_i(t)}{dt} = -\frac{\mathbf{V}_i(t) - \mathbf{v}(\mathbf{X}_i(t), t)}{\tau_d^i} + g\hat{\mathbf{z}}. \quad (6)$$

Here $\mathbf{v}(\mathbf{X}_i(t), t)$ is the fluid velocity at the particle position; $\tau_d^i(t) = \frac{R_i^2(t)}{3\nu\beta}$ is the particle response time (or Stokes time); $\beta = 3\rho_a/(\rho_a + 2\rho_w) \approx 3\rho_a/(2\rho_w)$ is the air/water density ratio; and g is the gravity acceleration. Equations (5) and (6), derived from the more general treatment of Maxey and Riley (1983), are valid for dilute suspensions of small spherical heavy particles. These hypothesis are well verified during the condensation stage, as discussed e.g. in Vaillancourt and Yau (2000).

Droplet statistics and dynamics in a turbulent medium can be studied by focusing on possibly many different features, see e.g. Pinsky and Khain (1997) for a review. Recently, also thanks to fundamental improvements in the laboratory tracking techniques (LaPorta et al. (2001); Mordant et al. (2001); Ayyalasomayajula et al. (2007)), progress in the understanding of particle motion in turbulence has undergone an explosive development. Together with the experimental efforts, theoretical analysis and numerical simulations have considered such different issues as particle acceleration statistics (see e.g. Ayyalasomayajula et al. (2007); Bec et al. (2006)), particle spatial inhomogeneous distribution (see e.g. Aliseda et al. (2002); Balkovsky et al. (2001); Collins and Keswani (2004); Bec et al. (2007)), collisional effects (see e.g. Wang et al. (2005); Wilkinson et al. (2006)). Granted that in the core of a warm cloud all these features can be relevant, here we focus on the particle size statistics during the early stages of the condensational growth.

3. Numerical simulations and range of parameters

As discussed earlier, DNS of cloud physics present a major problem: there is a huge number of degrees of freedom that cannot be described simultaneously. Turbulence is organized in spatial structures of typical scales ranging from the large scale L of hundreds of meters, down to the Kolmogorov scale η (typically 1 mm). Similarly, the timescales range from thousands to fractions of a second. Within this highly turbulent medium, a population of $10^{14} \div 10^{18}$ droplets evolve. Moreover, even if droplets are much smaller than any turbulent eddy, their trajectory spans the whole range of turbulent scales. This yields correlations with the fluctuations of the vapor field - see Celani et al. (2005, 2007) - and with the structures of the velocity field as shown, e.g., in Eaton and Fessler (1994). Therefore, turbulent motion at any scale plays a significant role in droplet dynamics. However, when dealing with experiments *in silico*, because of computational limitations, it is compulsory to choose a setting which describes only a limited range of fluctuations in the system.

Recent results, reported in Celani et al. (2005, 2007), of direct numerical simulations in two dimensions pointed out the importance of the large-scale fluctuations of the vapor field. These provide a strongly variable environment for droplet evolution resulting in a spreading of the droplet-size spectrum. In such context, the small scales of turbulence cannot be resolved and the analysis is limited to a statistically representative subset of the whole population of droplets. In Vaillancourt et al. (2002), the complementary setting is adopted: by concentrating on a small rising parcel, the authors can consistently describe the droplet evolution in full detail. This approach provides small fluctuations that eventually produce a limited degree of spreading. Note that the small scales inside a cloud are the endpoint of a wide turbulent cascade involving a huge range of interacting spatial and temporal scales. In particular, they are not independent from large scales, suggesting that approaches which separate small from large scales might fail

in reproducing turbulent effects. In this respect, since DNS do not describe the whole inertial range of turbulence, the fluid-parcel approach does not represent a small volume inside a huge cloud, but rather a very small cloud.

Here we wish to investigate how turbulence effects change with the Reynolds number by merging the two complementary approaches above mentioned. This is a crucial step in assessing the role of turbulence for cloud-droplet condensation, since real cloud turbulence has necessarily a dramatically higher Reynolds number than the simulated flows. To this purpose, we perform two series of direct numerical simulations at increasing resolution. The grid spacing Δx of each simulation corresponds to about 1 mm . By progressively increasing the number of grid points for each spatial direction, we can resolve larger integral scales L , defining the size of the cloud. More precisely, we consider two series of four numerical experiments, labeled as run (a), (b), (c) and (d), with 64^3 , 128^3 , 256^3 and 512^3 grid points respectively. The two series of simulations have different initial liquid water content (LWC): $\approx 1.2\text{ g/cm}^3$ for series 1 and $\approx 0.07\text{ g/cm}^3$ for series 2. The integral scale of the system varies from $L \sim 9\text{ cm}$ up to $L \sim 70\text{ cm}$. The microscale Reynolds numbers $Re_\lambda \approx \sqrt{15 Re}$ (see Frisch (1995)) range from $Re_\lambda \sim 40$ to $Re_\lambda \sim 185$, which represents the state-of-the-art for DNS in cloud physics. The ratio between the air kinematic viscosity and the vapor molecular diffusivity, also called the Schmidt number, is $Sc = \nu/\kappa = 1$, so that the flow and the scalar dissipative scales are of the same order. Table 2 lists all the relevant DNS parameters. Clearly the process of doubling the resolution, if iterated, would ideally lead to the description of the whole range of scales from $\eta \approx 1\text{ mm}$ to $L \approx 100\text{ m}$. As we can only perform the first few iterations of this process, the next step will be to discuss if this can be extrapolated to give information on Reynolds numbers which are not accessible by DNS. An attempt in this direction will be discussed at the end of next section with some detail.

For each DNS, equations (1) and (2) are integrated using pseudospectral methods with 2/3-rule de-aliasing (Orszag (1971)), in a three-periodic box. Molecular viscosity (and diffusivity) is chosen so as to match the Kolmogorov lengthscale with the grid spacing $\eta \simeq \delta x$: this choice ensures a good resolution of the small-scale dynamics. Kinetic energy is injected at an average rate ϵ , by keeping constant the total energy in each of the first two wavenumber shells (Chen et al. (1993)). The scalar field, also integrated on a triply periodic box, is forced by the assigned gradient A_1 ; the term $-s/\tau_s$ does not contribute as long as droplets are not injected into the flow. Time stepping is done using a 2^{nd} order Adam-Bashfort scheme and the time step is chosen to accurately resolve the smallest turbulent fluctuations and the particle acceleration.

We obtain a statistically stationary state for the velocity and supersaturation fields with no droplets by integrating equations (1) and (2) for few large-scale eddy turnover times $T_L = L/v_{rms}$. Figure 1 shows the supersaturation spectrum at the stationary state for run (d), $Re_\lambda \sim 200$, before particles injection. In agreement with classical Kolmogorov-Obukhov-Corrsin theory (see e.g. Tennekes and Lumley (1972)), this exhibits a $k^{-5/3}$ power law behavior in the Fourier space. Since the scalar spectrum is peaked on the large scales, as the integral scale increases, we approach larger and larger fluctuations. We indicate with σ_s^0 the supersaturation standard deviation in the stationary state before droplet injection. In the inset of Figure 1, we show that σ_s^0 increases linearly with the size of the system as expected from a dimensional balance of terms in equation (2), yielding $\sigma_s^0 \sim A_1 L$. Such increase can be understood from the physical viewpoint: larger cloud sizes correspond to larger displacements and stronger adiabatic

cooling. This directly provides larger fluctuations in the vapor field through the term $A_1 w$ in equation (2). Without the feedback coming from droplets' absorption of vapor, the value σ_s^0 would remain as in the stationary state, i.e. $\sigma_s^0 \sim A_1 L \sim A_1 w_{rms} T_L$.

Once the steady state has been attained, a monodispersed population of droplets (with initial radius $R_i = 13 \mu m$ for series 1 and $R_i = 5 \mu m$ for series 2) is injected into the flow. Droplet concentration is for all experiments $\approx 130 \text{ cm}^{-3}$, which means that, on average, about one out of $2 \div 4$ cells contains a droplet. In the largest simulation we followed the time evolution of 32 millions droplets. Initially, these are distributed randomly in space, according to a statistically homogeneous Poisson distribution. Lagrangian equations (5) and (6) for particle motion are integrated simultaneously with those for Eulerian fields (1) and (2). Particle initial velocities are set equal to the local fluid velocity ². To obtain droplet velocity from equation (6), the underlying flow velocity at the particle position has to be computed. This is done via a linear interpolation in the three spatial directions (Yeung and Pope (1988)), which was demonstrated to be adequate to obtain well-resolved particle acceleration. Similarly, we compute the vapor field $s(\mathbf{X}(t))$ at the particle position.

Coupling between droplets and the vapor field takes place via the term $-s/\tau_s$ of eq. (2), so that the initial vapor available is consumed for condensation onto droplet surface or released for droplet evaporation. In typical cloud conditions, τ_s is of order $1 \div 10 \text{ s}$, much smaller than typical large-scale eddy turnover times. As a result, the initial supersaturation standard deviation is depleted from $\sigma_s^0 \sim A_1 w_{rms} T_L$ to a lower value, that can be estimated by a dimensional analysis of equation (2): $\sigma_s^\infty \sim A_1 w_{rms} \tau_s$. We pointed out above that σ_s^0 grows with the size of the cloud and the Reynolds number: note that σ_s^∞ grows with Reynolds as well, since we can estimate $w_{rms} \sim v_\eta Re_\lambda^{1/2}$, where v_η is the velocity fluctuation at the viscous scale. Considering that $\sigma_s^\infty \sim \sigma_s^0 \tau_s / T_L$, the ratio between the large-scale eddy turnover time and the supersaturation absorption time is important to evaluate the supersaturation fluctuations available for condensation of cloud droplets. The complete system -flow, scalar and droplets- has been studied, at the largest resolution, for about two large-scale eddy turnover times. Longer time integrations were performed at lower resolutions.

4. Results and Discussion

Our simulations start with a spatially uniform Poissonian distribution of monodispersed droplets of radius $R_0 = 13 \mu m$ for series 1 and $R_0 = 5 \mu m$ for series 2, and with vanishing acceleration. As the cloud particles are released, they explore the entire volume and experience the range of vapor fluctuations available in the system, of initial standard deviation σ_s^0 . During an initial transient the fluctuations of the vapor field decrease due to the feedback of droplets. In Figure 2, the droplet square size distributions $P(R^2)$ are shown for runs (a)-(d) after one large-scale eddy turnover time for series 1 and series 2. A small degree of spreading is present for each simulation, increasing with the size of the cloud ³. This is due to the fact that - as already discussed above - larger domain sizes correspond to larger supersaturation fluctuations and longer large-scale eddy turnover times. In other words, when evolving in a larger cloud volume, droplets are exposed to more and more intense fluctuations of vapor, for longer and

²Tests have been performed by setting the droplet initial velocity equal to the terminal velocity $v_T = g\tau_d$. We did not observe any significant deviations in the results. Indeed particles rapidly equilibrate to the flow on a time scale of the order of their response time.

³Note that we impose a vanishing mean value for the initial supersaturation field, thus a constant mean droplet radius.

longer times. The knowledge of these characteristic times turns out to be crucial, as discussed in the sequel.

For $t \leq T_L$, the standard deviation σ_{R^2} of the square radii $R^2(t)$ increases linearly in time as shown in the inset of Figure 2. This means that at short time lags droplet surface grows with the vapor fluctuation initially experienced and does not feel the underlying local variations⁴. After few absorption times τ_s have elapsed, the vapor field standard deviation is depleted from σ_s^0 to σ_s^∞ , thus slowing down the broadening of droplet size distribution. The mean vapor absorption time, estimated through equation (3) with average concentration $\approx 130 \text{ drops cm}^{-3}$ and mean radius $13 \mu\text{m}$ and $5 \mu\text{m}$, turns out to be $\approx 2.5 \text{ s}$ for series 1 and $\approx 7 \text{ s}$ for series 2. Since this time scale is comparable with the eddy turnover time for simulations (a)-(d) (see table 1 and 2), the supersaturation fluctuations do not change considerably from their initial value during T_L . For this reason, the linear growth of σ_{R^2} in time extends to the whole large-scale eddy turnover time T_L and the final spreading, measured at $t = T_L$, is well approximated by:

$$\sigma_{R^2}(T_L) \sim 2A_3\sigma_s^0 T_L. \quad (7)$$

The square radius standard deviation $\sigma_{R^2}(T_L)$ is found to be similar for the two series of simulations, pointing once more to a limited role of vapor absorption by condensation when the Reynolds number is small and $\tau_s \approx T_L$.

In Figure 3, the standard deviation $\sigma_{R^2}(T_L)$ is shown as a function of the microscale Reynolds number Re_λ characterizing flows (a), (b), (c) and (d). We immediately observe that the final broadening grows with the Reynolds number for both series of simulations. Given the following dimensional relations $T_L \sim \tau_\eta Re_\lambda$, $w_{rms} \sim v_\eta Re_\lambda^{1/2}$ and $\sigma_s^0 \sim A_1 w_{rms} T_L$, it is straightforward to translate the simple expectation (7) in a scaling relation with the Reynolds number:

$$\sigma_{R^2} \sim A_3 A_1 v_\eta \tau_\eta^2 Re_\lambda^{5/2}, \quad (8)$$

based on self-similarity of the growth process during the turbulent regime. In Figure 3 we show for comparison the dimensional expectation (8).

It is natural to wonder whether this trend can give information on the final broadening achieved at Reynolds numbers higher than $Re_\lambda = 200$. This delicate point deserves insight since the Reynolds number of real cloud turbulence typically achieve huge values that cannot be described by direct numerical simulations.

At larger Reynolds number and large-scale eddy turnover times, droplets significantly absorb the surrounding vapor, so that σ_s^0 is no longer a good approximation of σ_s . This means that the scaling (8) is an upper bound for the actual spectral broadening at larger Reynolds number. A lower bound can be simply obtained by replacing the supersaturation fluctuations with their long time value $\sigma_s^\infty \sim \sigma_s^0 \tau_s / T_L$, yielding a correction to the upper bound (8) of a factor τ_s / T_L . Note that the scaling relation in (8) would also change into a slower growth of the final broadening with the Reynolds number, proportional to $Re_\lambda^{3/2}$.

The ratio τ_s / T_L fluctuates both in space and time according to the local properties of both turbulence and droplet population. Given the Kolmogorov timescale, we can estimate the large-scale eddy turnover time at larger Reynolds numbers through $T_L \sim \tau_\eta Re_\lambda$, as mentioned above. For a cloud of typical size $L \sim 100 \text{ m}$, liquid water content LWC 1.2 g/m^3 with

⁴A proportional linear growth is also observed for the standard deviation of droplet radii $R(t)$, (not shown). This is because, given the tiny supersaturation fluctuations, the droplet-size distribution is close to a Gaussian and the mean radius is much larger than the standard deviation. Hence $\sigma_{R^2}^2 \approx 2\sigma_R^4 + 4\sigma_R^2 \langle R \rangle^2 \approx 4\sigma_R^2 \langle R \rangle^2$.

130 drops cm^{-3} and Reynolds number⁵ $Re_\lambda \sim (4000 \div 7000)$, the large-scale eddy turnover time is $T_L \approx 150$ s while τ_s does not depend on Reynolds and its mean value is $\tau_s \approx 2.5$ s, as in series 1. The extrapolation of the upper bound (8) together with the lower bound gives: $(3.3 \pm 1.6)\mu m^2 < \sigma_{R^2}(T_L) < (200 \pm 100)\mu m^2$.

Validating these predictions by a direct numerical simulation, describing the proper number of droplets and the whole range of space-time scales involved, is of course not possible. Instead, we present a direct numerical simulation, labeled run (e), designed so as to reproduce the large-scale parameters typical of a cloud of size $L = 100$ m: $T_L \approx 150$ s, $\sigma_s^0 \approx 2\%$, $v_{rms} \approx 0.6$ m s⁻¹, $L \approx 100$ m. The goal of this further experiment is to verify that at long space and time scales (T_L is now much larger than τ_s), the lower bounds on vapor fluctuations σ_s and on the square radius fluctuations σ_{R^2} become more relevant. Of course, the small-scale parameters do not match the realistic ones: in this run the smallest resolved scales are $\eta \approx 25$ cm and $\tau_\eta \approx 4$ s, and the turbulence Reynolds number is $Re_\lambda = 185$. The initial radius of droplets is 13 μ m and the numerical resolution is $N^3 = 256^3$ grid points. Space-time integration of the system has the same features described in Section 3, and reference values for the physical parameters entering the model equations are those listed in Table 1.

Clearly, we can not follow the evolution of 130 cm^{-3} droplets, since in a volume of $(100)^3$ m³ they would sum up to $N^* = 1.3 \times 10^{14}$. The traditional cloud physics approach avoids this problem by focusing on a number density function representing the local concentration of droplets with a given size (see e.g. Andrejczuk et al. (2004); Jeffery et al. (2007)). However, a complete continuous description for the turbulent transport of inertial particles is still an open issue (see Boffetta et al. (2007) and references therein). Though more computationally demanding, a Lagrangian approach turns out to be more appropriate. We choose then to consider the complete evolution of a subset N_{drops} of droplets, representative of the whole population. Of course, the whole population would absorb for condensation more vapor than the representative subset does. Therefore an algorithm is needed to account for the correct feedback of droplets on the supersaturation field. In order to accomplish this task, we simply normalize the field τ_s with a factor N^*/N_{drops} . Details on the meaning and the convergence of this simple algorithm are discussed in appendix B.

The supersaturation fluctuations for simulation (e) start with $\sigma_s^0 \sim A_1 w_{rms} T_L \approx 2\%$; after few vapor absorption times they are depleted to $\sigma_s^\infty \approx 0.04\%$ and oscillate around this value for all later times. The relevant spreading of the square size distribution shown in Figure 4 can be quantified in terms of the standard deviation of the radius and of the square radius. After one large-scale eddy turnover time, we obtain $\sigma_R(T_L) \simeq (0.30 \pm 0.04)$ μ m and $\sigma_{R^2}(T_L) \simeq (7 \pm 1)$ μ m², respectively. Although simulation (e) cannot resolve the whole range of spatial scales of turbulence, by matching the parameters on the large scales of the problem it is able to reproduce the intensity of the large-scale fluctuations.

The final spreading achieved is very close to the lower bound, obtained above by assuming that the supersaturation fluctuations stabilize to σ_s^∞ and rapidly forget their initial condition. This is consistent with the picture drawn and supports the observation that the lower bound is more relevant when dealing with large space-time scales. The result suggests that this could be the case for large Reynolds number turbulence. Let us remark however that care must be taken in this respect, since the spatio-temporal complexity of turbulence at $Re_\lambda \approx 5000$ is not described by the direct numerical simulation (e) presented.

⁵To put errorbars on the Reynolds number we consider fluctuations of 25% on the average value, the same level of fluctuation observed in simulation runs (a)-(d).

5. Conclusion and Perspectives

Turbulent fluctuations have been shown to play a role for the broadening of the droplet-size distribution in an idealized setting for condensation in warm adiabatic cloud cores. A qualitative explanation for this observation relies on the non-trivial spatial structure of turbulent fields where droplets collect strongly different histories. The droplet size spectra broadening is shown to depend on the actual range of spatial scales characterizing the turbulent structure of the fields. In particular, we show an increase of broadening with the microscale Reynolds number by means of two series of direct numerical simulations up to $Re_\lambda \sim 200$ and with millions of droplets.

The general outcome of this result is that the role of turbulence for condensation in clouds may not be assessed just by focusing on small Reynolds numbers, where a limited range of spatial scales is considered. Therefore, a strategy must be conceived to extrapolate the results of DNS or laboratory experiments, that cannot achieve the huge Reynolds numbers of real cloud turbulence. This is also the case for fluid parcel models which in fact do not represent a portion of a large cloud, but rather a very small cloud. Indeed, it is well-known that initially close droplets inside a parcel would not remain close for a long time, but separate explosively due to turbulent transport.

In particular, though at the Reynolds numbers considered the broadening is relatively small, it may potentially achieve relevant values at the huge Reynolds numbers of real cloud turbulence. In order to get a better intuition on this potential, we perform a dimensional analysis of the final broadening viewed as a function of the Reynolds number. At moderate Reynolds numbers, it is possible to neglect the feedback of droplets on the vapor field. This yields a dimensional expectation consistent with the DNS data.

At larger Reynolds numbers, however, droplets are expected to consistently modify the surrounding vapor field. Therefore, the extrapolation of the dimensional behavior provides an upper bound to the actual spectral broadening at large Reynolds numbers. A correction is proposed to estimate the effective absorption of vapor for condensation at large Reynolds numbers, yielding a lower bound on the spectral broadening. A further simulation designed to discuss the validity of this argument shows that at large space-time scales the behavior is well approximated by the lower bound. This suggests, within the limits of simple dimensional arguments, that the lower bound could be a good candidate to estimate the size-spectra broadening at large Reynolds numbers.

In this work, we focused on the role of turbulence for droplet condensation at moderate-high Reynolds numbers. In order to enlighten the basic mechanisms yielded by turbulence, we considered a simple model describing the essential physical processes. More sophisticated models have been proposed in the literature accounting for additional microphysical and thermodynamic couplings. Ingredients such as the explicit dependence of the vapor field on the temperature fluctuations, the microscopic interactions of droplets with the turbulent fields and the role of buoyancy both at small and large scales may yield corrections to the presented results. Other aspects, such as droplet preferential concentration and modified relative velocity effects, were not specifically addressed in this work, though they are in fact included in the model. These have been associated to the efficiency of collision/coalescence processes (see Wang et al. (2005); Wilkinson et al. (2006)), before they become dominated by gravity.

The problem here considered clearly deserves further theoretical, experimental and numerical insight and represents a promising challenge for future research. In particular, the ideas at the basis of this work could be well explored through laboratory experiments. The higher Reynolds

numbers covered would allow to verify and complement the picture drawn through the numerical analysis presented.

Acknowledgments.

We acknowledge discussions with Antonio Celani and Andrea Mazzino, who have inspired and motivated this work. AS was partially supported by L'Oréal Italia - Unesco For Women in Science Fellowship, and by HPC-Europa Transnational Acces Program. AL acknowledges discussions with Andrea Buzzi and support from CNR grant "Short-Term Mobility". Numerical simulations were performed at the supercomputing center CINECA (Italy). Raw data from our numerical simulations can be downloaded freely from the web site of the iCFDdatabase [HTTP://CFD.CINECA.IT](http://CFD.CINECA.IT).

APPENDIX A

Water-vapor interaction

The expression of the absorption time τ_s can be computed directly from the classical form of Twomey's model by identifying the terms:

$$\frac{s}{\tau_s} = A_2 \frac{d\rho_L}{dt}, \quad \text{where} \quad A_2 = \frac{R_a T}{\varepsilon_{wa} e_s} + \frac{\varepsilon_{wa} \mathcal{L}^2}{p T c_{pa}} \quad (\text{A1})$$

where $\rho_L = m_w/V$ is the density of liquid water of mass m_w inside volume V ; ε_{wa} is the ratio between the molecular weight of water and dry air; \mathcal{L} is the latent heat of water evaporation; R_a is the specific gas constant for dry air; T is the absolute temperature and c_{pa} is the specific heat of dry air at constant pressure p (see Pruppacher and Klett (1997)). The evaluation of the constant A_2 in typical warm cloud conditions gives the reference value shown in Table 1. Its fluctuations with temperature are less than 1%, so that we assume A_2 to be constant. Since we focus on inner cloud cores, we neglect entrainment; then droplets inside the volume V are the only responsible for the local change in vapor content:

$$\frac{d\rho_L}{dt} = \frac{1}{V} \frac{dm_w}{dt} = \frac{1}{V} \sum_{i=1}^n 4\pi \rho_w R_i^2 \frac{dR_i}{dt} = \frac{4\pi \rho_w A_3}{V} \sum_{i=1}^n R_i s, \quad (\text{A2})$$

where (see eq. (13-28) of Pruppacher and Klett (1997), ignoring small curvature and solute terms for activated droplets),

$$A_3 = \left(\frac{R_v T}{\rho_w D_v e_s} + \frac{\mathcal{L}^2}{\rho_w k_a R_v T^2} \right)^{-1}, \quad (\text{A3})$$

where R_v is the specific gas constant for moist air, ρ_w is the density of water, D_v is the thermal diffusivity of water vapor in air, and k_a is the air thermal conductivity.

In eq. (A2), R_i are the radii of the n droplets inside the volume V . The rate of variation of the radius is given by equation (4), where s is considered equal for each droplet inside the small volume V . In the numerical analysis, V is a cube of edge η , similar to the vapor diffusive scale. The fluctuations of the scalar field are tiny under this scale and all the droplets inside the volume V experience approximately the same value of s . In this sense, the Twomey's parcel, where no spatial fluctuations of the supersaturation field are accounted for, corresponds to our grid cell. From equations (A1) and (A2) we end up with the expression (3) for the absorption time τ_s .

APPENDIX B

Renormalization of droplets population

Simulation (e) is designed to describe a volume of $(100\text{ m})^3$ with 130 cm^{-3} droplets. A major drawback of this simulation is that it can not describe turbulence structure at the smallest scales, below $\eta = 25\text{ cm}$ and $\tau_\eta = 4\text{ s}$. Also it can not follow the individual history of the correct number of droplets. This might influence the statistics of vapor fluctuations since the correct feedback of droplets on the vapor field is not accounted for. In particular, a concentration of 130 cm^{-3} droplets yields $N^* \approx 10^{14}$ total number of particles, whereas we consider the evolution of several millions droplets (N_{drops}) due to computational limits. Clearly, 10^{14} droplets would absorb much more vapor for condensation than a few millions do, thus an algorithm is needed in order to account for this. The simplest way to estimate the feedback of the whole population on the supersaturation field is to normalize τ_s with a factor N_{drops}/N^* . This amounts to consider each droplet as representative of N^*/N_{drops} *equal* particles in the same volume $(\delta x)^3$, where $\delta x \approx 25\text{ cm}$.

To evaluate the reliability of this approach, we must consider the single grid cell. If there is 1 representative drop per cell, the algorithm computes the feedback on vapor as if the average size of droplets in the cell was exactly the radius of that unique representative. On the contrary, a volume of $(25\text{ cm})^3$ - the grid cell size in simulation (e)-, should contain several droplets spanning a whole size spectrum whose mean value is not well represented by one single droplet. Of course, a higher number of particles would better represent the local mean radius and we expect the algorithm to converge for density values larger than 1 droplet per cell. We test this expectation, by repeating simulation (e) for a time lag $t = T_L/4$, with 0.4, 1, 3 and 6 droplets per grid cell, which correspond to a total number of $N_{\text{drops}} \approx 7, 17, 50$ and 100 millions droplets, respectively. Consistently, we use different renormalization factors N^*/N_{drops} . On average, the supersaturation absorption timescale τ_s is the same in the four simulations (not shown), pointing to a correct renormalization.

In figure 5, left panel, the four standard deviations of the supersaturation field are shown in time. They all start with the same initial value (about $A_1 w_{rms} T_L \approx 2\%$ - not shown), and relax to a value of the order of $A_1 w_{rms} \tau_s$, with some differences for the different concentrations of representative droplets. These deviations decrease when the number of representative droplets increases, showing that the algorithm renormalizing the feedback of droplets on vapor converges. Consistently, the evolution of the size spectra broadening (shown in figure 5, right panel) tends to collapse to a unique curve when the number of droplets per cell is larger than 1. According to this analysis, we choose to perform the complete simulation lasting one large-scale eddy turnover time with 1 and 3 droplets per cell, which correspond to a total number of about 17 and 50 millions droplets, respectively. The error bar on the final broadening is estimated from these two runs.

References

- Aliseda, A., A. Cartellier, F. Hainaux, and J. C. Lasheras, 2002: Effect of preferential concentration on the settling velocity of heavy particles in homogeneous isotropic turbulence. *J. Fluid Mech.*, **468**, 77.
- Andrejczuk, M., W. W. Grabowski, S. P. Malinowski, and P. K. Smolarkiewicz, 2004: Numerical simulations of cloud-clear air interfacial mixing. *J. Atmos. Sci.*, **61**, 1726–1739.
- Ayyalasomayajula, S., A. Gylfason, and Z. Warhaft, 2007: Lagrangian measurements of fluid and inertial particles in decaying grid generated turbulence. in *Proceedings of the IUTAM Symposium on Computational Physics and New Perspectives in Turbulence*, 2006, **2**, 171–175.
- Balkovsky, E., G. Falkovich, and A. Fouxon, 2001: Intermittent distribution of inertial particles in turbulent flows. *Phys. Rev. Lett.*, **86**, 2790.
- Bartlett, J. T. and P. R. Jonas, 1972: On the dispersion of the size of droplets growing by condensation in turbulent clouds. *Quart. J. Roy. Meteor. Soc.*, **98**, 150–164.
- Bec, J., L. Biferale, G. Boffetta, A. Celani, M. Cencini, A. Lanotte, S. Musacchio, and F. Toschi, 2006: Acceleration statistics of heavy particles in turbulence. *J. Fluid. Mech.*, **550**, 349.
- Bec, J., L. Biferale, M. Cencini, A. Lanotte, S. Musacchio, and F. Toschi, 2007: Heavy particle concentration in turbulence at dissipative and inertial scales. *Phys. Rev. Lett.*, **98**, 084 502.
- Blyth, A., 1993: Entrainment in cumulus clouds. *J. Appl. Meteorol.*, **32**, 626–641.
- Boffetta, G., A. Celani, F. D. Lillo, and S. Musacchio, 2007: The eulerian description of dilute collisionless suspension. *Europhys. Lett.*, **78**, 14 001.
- Brenguier, J. L. and L. Chaumat, 2001: Droplet spectra broadening in cumulus clouds. part i. broadening in adiabatic cores. *J. Atmos. Sci.*, **58**, 628–641.
- Celani, A., G. Falkovich, A. Mazzino, and A. Seminara, 2005: Droplet condensation in turbulent flows. *Europhys. Lett.*, **70**, 775–782.
- Celani, A., A. Mazzino, A. Seminara, and M. Tizzi, 2007: Droplet condensation in convective turbulence. *Journ. Turb.*, **8**, 1–9.
- Chen, S., G. D. Doolen, R. H. Kraichnan, and Z. S. She, 1993: On the statistical correlations between velocity increments and locally averaged dissipation in homogeneous turbulence. *Phys. Fluids A*, **5**, 458–463.
- Collins, L. R. and A. Keswani, 2004: Reynolds number scaling of particle clustering in turbulent aerosol. *New J. Phys.*, **6**, 119.
- Eaton, J. K. and J. R. Fessler, 1994: Preferential concentrations of particles by turbulence. *Int. J. Multiphase Flow*, **20**, 169 209.

- Falkovich, G., A. Fouxon, and M. G. Stepanov, 2002: Acceleration of rain initiation by cloud turbulence. *Nature*, **419**, 151–154.
- Frisch, U., 1995: *Turbulence*. Cambridge University Press, Cambridge, UK.
- Ghosh, S., J. Davila, J. C. R. Hunt, A. Srdic, H. J. S. Ferrando, and P. R. Jonas, 2005: How turbulence enhances coalescence of settling particles with applications for rain in clouds. *Proc. Roy. Soc. A*, **461**, 3059–3088.
- IPCC-WGI, 2001: *Climate Change 2001: the scientific basis*. Cambridge University Press, Cambridge UK and New York, NY, USA, contribution of working group I to the third assessment report of the intergovernmental panel on climate change.
- Jeffery, C. A., J. M. Reisner, and M. Andrejczuk, 2007: Another look at stochastic condensation. *J. Atmos. Sci.*, **64**, 3949–3968.
- Johnson, D. B., 1982: The role of giant and ultragiant aerosol particles in warm rain initiation. *J. Atmos. Sci.*, **39**, 448–460.
- Korczyk, P., P. Malinowski, and T. A. Kowalewski, 2006: Mixing of cloud and clear air in centimeter scales observed in laboratory by means of particle image velocimetry. *Atmos. Res.*, **82**, 173–182.
- Korolev, A. V., 1995: The influence of supersaturation fluctuations on droplet size spectra formation. *J. Atmos. Sci.*, **52**, 3620–3634.
- Korolev, A. V. and I. P. Mazin, 2003: Supersaturation of water vapor in clouds. *J. Atmos. Sci.*, **60**, 2957–2974.
- LaPorta, A., G. A. Voth, A. M. Crawford, J. Alexander, and E. Bodenschatz, 2001: Fluid particle accelerations in fully developed turbulence. *Nature*, **409**, 1017.
- Lee, I. Y. and H. R. Pruppacher, 1977: A comparative study on the growth of cloud drops by condensation using an air parcel model with and without entrainment. *Pure and Appl. Geophys.*, **115**, 523–545.
- Levin, L. M. and Y. S. Sedunov, 1966: Stochastic condensation of drops and kinetics of cloud spectrum formation. *J. Rech. Atmos.*, **2**, 425–432.
- Malinowski, S. P., I. Zawadzki, and P. Banat, 1998: Laboratory observations of cloud clear air mixing in small scales. *J. Atmos. Ocean. Technol.*, **15**, 1060–1065.
- Martonen, T. B., (Ed.) , 2000: *Medical Applications of Computer Modelling: Cardiovascular and Ocular System*. WIT PRESS, UK.
- Maxey, M. R. and J. Riley, 1983: Equation of motion of a small rigid sphere in a nonuniform flow. *Phys. Fluids*, **26**, 883–889.
- Mazin, I. P., 1968: The stochastic condensation and its effects on the formation of cloud droplet size distribution. *Proc. Int. Conf. on Cloud Physics, Toronto, ON, Canada*.

- Mordant, N., P. Metz, O. Michel, and J.-F. Pinton, 2001: Measurement of lagrangian velocity in fully developed turbulence. *Phys. Rev. Lett.*, **87**, 214 501.
- Orszag, S., 1971: On the elimination of aliasing in finite difference schemes by filtering high-wavenumber components. *J. Atmos. Sci.*, **28**, 1074.
- Pruppacher, H. R. and J. D. Klett, 1997: *Microphysics of Clouds and Precipitation*. Kluwer Academic Publishers, Boston, MA.
- Saffman, P. G. and J. S. Turner, 1956: On the collision of drops in turbulent cloud. *J. Fluid Mech.*, **1**, 16–30.
- Shaw, R. A., 2003: Particle-turbulence interactions in atmospheric clouds. *Annu. Rev. Fluid Mech.*, **35**, 183–227.
- Shaw, R. A., W. C. Reade, L. R. Collins, and J. Verlinde, 1998: Preferential concentration of cloud droplets by turbulence: Effects on the early evolution of cumulus cloud droplet spectra. *J. Atmos. Sci.*, **55**, 1965–1976.
- Squires, P., 1952: The growth of cloud drops by condensation. *Aust. J. Sci. Res.*, **5**, 59–86.
- Stevens, B., 2005: Atmospheric moist convection. *Annu. Rev. Earth Planet. Sci.*, **33**, 605–643.
- Sundaram, S. and L. R. Collins, 1997: Collision statistics in an isotropic particle-laden turbulent suspension. part i. direct numerical simulations. *J. Fluid. Mech.*, **335**, 75–109.
- Tennekes, H. and J. L. Lumley, 1972: *A first course in turbulence*. MIT press, Cambridge, MA.
- Twomey, S., 1959: The nuclei of natural cloud formation. part ii. the supersaturation in natural clouds and the variation of cloud droplet concentration. *Geophys. Pure Appl.*, **43**, 243–249.
- Vaillancourt, P. A. and M. K. Yau, 2000: Review of particle-turbulence interactions and consequences for cloud physics. *Bull. Am. Meteor. Soc.*, **81**, 285–298.
- Vaillancourt, P. A., M. K. Yau, P. Bartello, and W. W. Grabowski, 2002: Microscopic approach to cloud droplet growth by condensation. part ii: Turbulence, clustering and condensational growth. *J. Atmos. Sci.*, **59**, 3421–3435.
- Vaillancourt, P. A., M. K. Yau, and W. W. Grabowski, 2001: Microscopic approach to cloud droplet growth by condensation. part i: Model description and results without turbulence. *J. Atmos. Sci.*, **58**, 1945–1964.
- Wang, L.-P., A. Orlando, S. Kasprzak, and W. W. Grabowski, 2005: Theoretical formulation of collision rate and collision efficiency of hydrodynamically interacting cloud droplets in turbulent atmosphere. *J. Atmos. Sci.*, **62**, 2433.
- Wang, L. P., Y. Xue, O. Ayala, and W. W. Grabowski, 2006: Effects of stochastic coalescence and air turbulence on the size distribution of cloud droplets. *Atmos. Res.*, **82**, 416–432.
- Warner, J., 1969: The microstructure of cumulus clouds. part i. general features of the droplet spectrum. *J. Atmos. Sci.*, **26**, 1049–1059.

- Wilkinson, M., B. Mehlig, and V. Bezuglyy, 2006: Caustic activation of rain showers. *Phys. Rev. Lett.*, **97**, 048 501.
- Yeung, P. K. and S. B. Pope, 1988: An algorithm for tracking fluid particles in numerical simulations of homogeneous turbulence. *J. Comput. Phys.*, **79**, 373–416.
- Zhao, F., M. C. Lai, and D. L. Harrington, 1999: Automotive spark-ignited direct-injection gasoline engines. *Prog. in Ener. and Comb. Sci.*, **25**, 437–562.

List of Figures

- 1 Log-log plot of the stationary supersaturation spectrum for the run (d) at $Re_\lambda \sim 200$. It shows a $k^{-5/3}$ power law behavior, as expected from Kolmogorov-Obukhov-Corssin theory. The turbulent velocity field also displays a Kolmogorov spectrum (not shown). Inset: log-log plot of the standard deviation of the supersaturation field σ_s^0 , measured in the stationary state, versus the size of the system L . The behavior is in agreement with the dimensional prediction $\sigma_s^0 \sim A_1 L$ 20
- 2 Droplet square size distribution $P(R^2)$ measured after one large-scale eddy turnover time T_L , for the 4 DNS of series 1 (left panel) and series 2 (right panel). At increasing the turbulence Reynolds number, we move from inner to outer curves. Symbols: run (a) red triangles; run (b) green dots; run (c) blue circles and run (d) purple squares. In each run, droplets' initial size distribution (not shown) is $\delta(R - R_0)$, with $R_0 = 13 \mu m$ for series 1 and $R_0 = 5 \mu m$ for series 2. Each simulation presents a small degree of spreading, which increases with the Reynolds number. Inset: log-log plot of the time evolution of the standard deviation of the square size distribution σ_{R^2} for the runs (a)-(d) (from bottom to top). Symbols are the same of the main frame. 21
- 3 Log-log plot of the spreading of droplet size distribution $\sigma_{R^2}(T_L)$ for the square radius R^2 , measured after one large-scale eddy turnover time T_L , as a function of the Reynolds number Re_λ . Data refer to simulations (a)-(d) of series 1 (red squares) and series 2 (green circles). For both series, the spreading is larger as the Reynolds number increases, since droplets evolve in conditions which are more and more differentiated. The dimensional prediction $\sigma_{R^2} \sim c_1 Re_\lambda^\xi$ with $\xi = 5/2$, $c_1 \propto A_1 A_3 v_\eta \tau_\eta^2$ is shown for comparison (see the text). The extrapolation of this law gives an upper bound to the final spreading for the target cloud of parameters $L = 100 m$, $\sigma_s^0 \sim 2\%$ and $Re_\lambda \sim 4000 \div 7000$: $\sigma_{R^2}^{ext} \sim (200 \pm 100) \mu m^2$. A correction of the expectation accounting for vapor depletion due to droplet feedback gives $\sigma_{R^2}^{ext} \sim (3.3 \pm 1.6) \mu m^2$ for series 1, and $\sigma_{R^2}^{ext} \sim (9.3 \pm 4.5) \mu m^2$ for series 2 (see the text). 22
- 4 Droplet square size distribution $P(R^2)$ measured after one large-scale eddy turnover time $T_L \sim 150 s$ for run (e), matching the large scale cloud parameters. In the inset, time evolution of the standard deviation of the radius distribution, $\sigma_R(t)$, and of the square radius distribution, $\sigma_{R^2}(t)$. At time $t = T_L$, we measure $\sigma_R(T_L) \simeq (0.30 \pm 0.04) \mu m$ and $\sigma_{R^2}(T_L) \simeq (7 \pm 1) \mu m^2$ 23
- 5 Left panel: Supersaturation standard deviation as a function of time. Right panel: Droplet-square-radius standard deviation σ_{R^2} as a function of time. Results are shown for simulation (e), with 4 different numbers of droplets N_{drops} representative of a population of $N^* \approx 10^{14}$ droplets. The feedback of the whole population on the supersaturation field is accounted for by renormalizing τ_s with a factor N^*/N_{drops} (see text). The algorithm converges when the number of representative droplets is larger than $1/cell$ 24

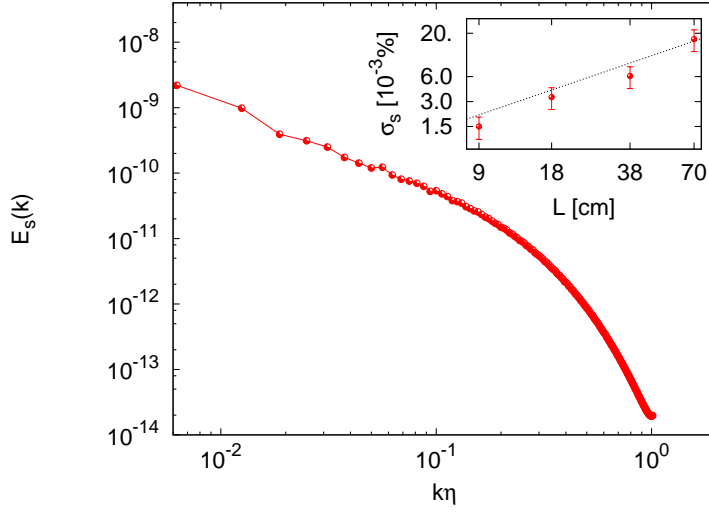


FIG. 1. Log-log plot of the stationary supersaturation spectrum for the run (d) at $Re_\lambda \sim 200$. It shows a $k^{-5/3}$ power law behavior, as expected from Kolmogorov-Obukhov-Corssin theory. The turbulent velocity field also displays a Kolmogorov spectrum (not shown). Inset: log-log plot of the standard deviation of the supersaturation field σ_s^0 , measured in the stationary state, versus the size of the system L . The behavior is in agreement with the dimensional prediction $\sigma_s^0 \sim A_1 L$.

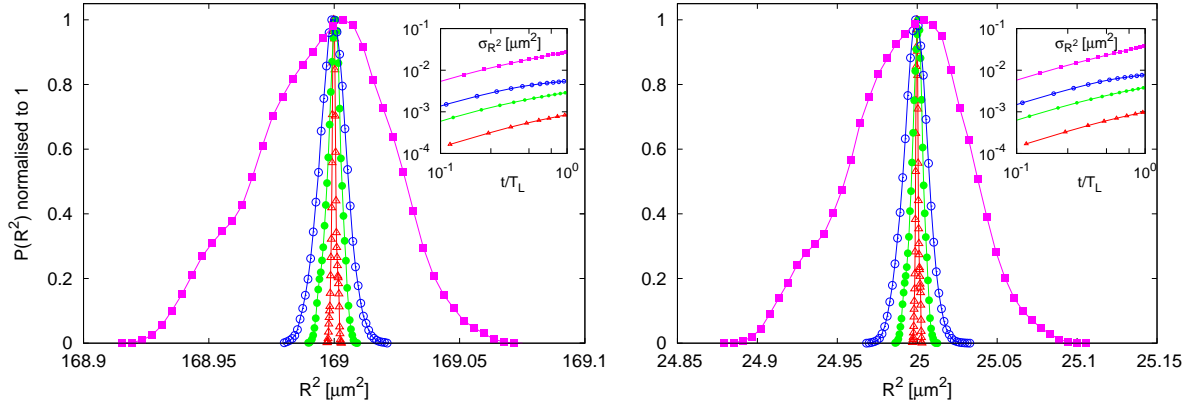


FIG. 2. Droplet square size distribution $P(R^2)$ measured after one large-scale eddy turnover time T_L , for the 4 DNS of series 1 (left panel) and series 2 (right panel). At increasing the turbulence Reynolds number, we move from inner to outer curves. Symbols: run (a) red triangles; run (b) green dots; run (c) blue circles and run (d) purple squares. In each run, droplets' initial size distribution (not shown) is $\delta(R - R_0)$, with $R_0 = 13 \mu m$ for series 1 and $R_0 = 5 \mu m$ for series 2. Each simulation presents a small degree of spreading, which increases with the Reynolds number. Inset: log-log plot of the time evolution of the standard deviation of the square size distribution σ_{R^2} for the runs (a)-(d) (from bottom to top). Symbols are the same of the main frame.

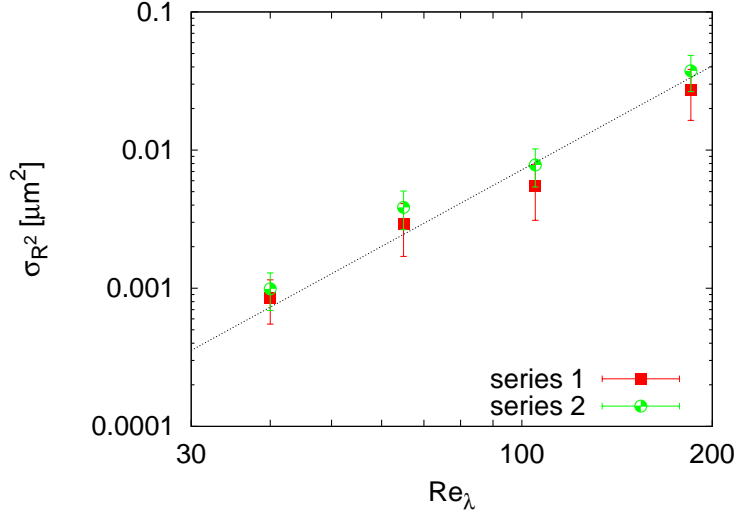


FIG. 3. Log-log plot of the spreading of droplet size distribution $\sigma_{R^2}(T_L)$ for the square radius R^2 , measured after one large-scale eddy turnover time T_L , as a function of the Reynolds number Re_λ . Data refer to simulations (a)-(d) of series 1 (red squares) and series 2 (green circles). For both series, the spreading is larger as the Reynolds number increases, since droplets evolve in conditions which are more and more differentiated. The dimensional prediction $\sigma_{R^2} \sim c_1 Re_\lambda^\xi$ with $\xi = 5/2$, $c_1 \propto A_1 A_3 v_\eta \tau_\eta^2$ is shown for comparison (see the text). The extrapolation of this law gives an upper bound to the final spreading for the target cloud of parameters $L = 100 m$, $\sigma_s^0 \sim 2\%$ and $Re_\lambda \sim 4000 \div 7000$: $\sigma_{R^2}^{ext} \sim (200 \pm 100) \mu m^2$. A correction of the expectation accounting for vapor depletion due to droplet feedback gives $\sigma_{R^2}^{ext} \sim (3.3 \pm 1.6) \mu m^2$ for series 1, and $\sigma_{R^2}^{ext} \sim (9.3 \pm 4.5) \mu m^2$ for series 2 (see the text).

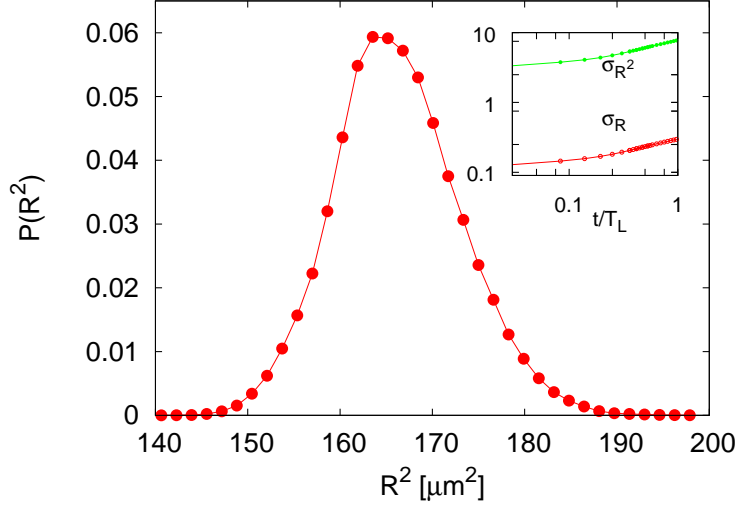


FIG. 4. Droplet square size distribution $P(R^2)$ measured after one large-scale eddy turnover time $T_L \sim 150$ s for run (e), matching the large scale cloud parameters. In the inset, time evolution of the standard deviation of the radius distribution, $\sigma_R(t)$, and of the square radius distribution, $\sigma_{R^2}(t)$. At time $t = T_L$, we measure $\sigma_R(T_L) \simeq (0.30 \pm 0.04) \mu m$ and $\sigma_{R^2}(T_L) \simeq (7 \pm 1) \mu m^2$.

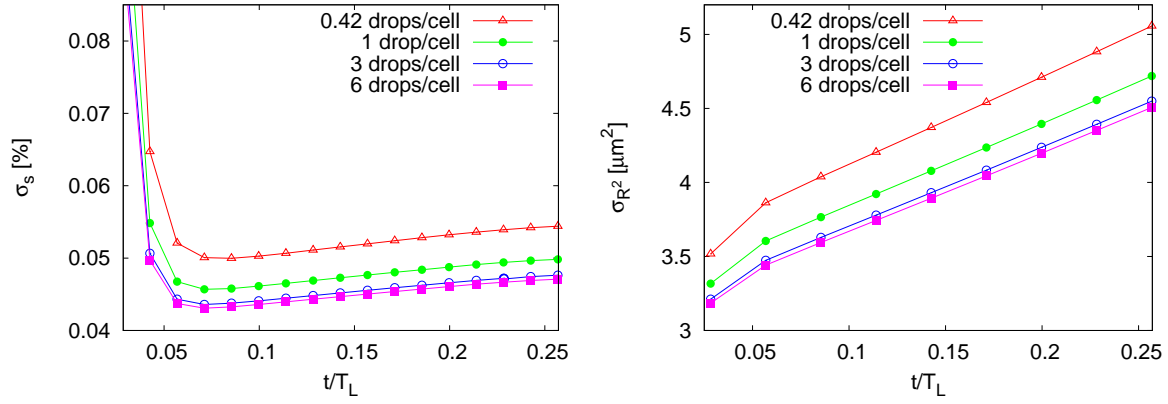


FIG. 5. Left panel: Supersaturation standard deviation as a function of time. Right panel: Droplet-square-radius standard deviation σ_{R^2} as a function of time. Results are shown for simulation (e), with 4 different numbers of droplets N_{drops} representative of a population of $N^* \approx 10^{14}$ droplets. The feedback of the whole population on the supersaturation field is accounted for by renormalizing τ_s with a factor N^*/N_{drops} (see text). The algorithm converges when the number of representative droplets is larger than $1/cell$.

List of Tables

1	Reference values for the physical parameters used in the numerical experiments. A_1 is the global supersaturation gradient. A_2 and A_3 are functions of the ambient thermodynamic parameters (see appendix A): as reference values for the temperature and pressure we used $T = 283K$ and $p \approx 1000hPa$. The values of the vapor relaxation time τ_s , the droplet radius R and the Stokes number St correspond to averages on the initial condition of droplet population.	26
2	Parameter of the DNS, series 1 and 2. From left to right: number of gridpoints N^3 , integral scale L , large-scale eddy turnover time T_L , microscale Reynolds number Re_λ , average kinetic energy dissipation rate ϵ , Kolmogorov spatial scale η , Kolmogorov timescale τ_η , initial supersaturation standard deviation σ_s^0 , velocity standard deviation v_{rms} and number of droplets N_{drops}	27

TABLE 1. Reference values for the physical parameters used in the numerical experiments. A_1 is the global supersaturation gradient. A_2 and A_3 are functions of the ambient thermodynamic parameters (see appendix A): as reference values for the temperature and pressure we used $T = 283K$ and $p \approx 1000hPa$. The values of the vapor relaxation time τ_s , the droplet radius R and the Stokes number St correspond to averages on the initial condition of droplet population.

<i>label</i>	A_1 (m^{-1})	A_2 ($kg^{-1}m^3$)	A_3 ($\mu m^2 s^{-1}$)	N_{drops}/V (cm^{-3})	LWC (g/m^3)	τ_s (s)	R (μm)	St
<i>series 1</i>	5×10^{-4}	350	50	130	1.2	2.5	13	3.5×10^{-2}
<i>series 2</i>	5×10^{-4}	350	50	130	0.07	7	5	5×10^{-3}

TABLE 2. Parameter of the DNS, series 1 and 2. From left to right: number of gridpoints N^3 , integral scale L , large-scale eddy turnover time T_L , microscale Reynolds number Re_λ , average kinetic energy dissipation rate ϵ , Kolmogorov spatial scale η , Kolmogorov timescale τ_η , initial supersaturation standard deviation σ_s^0 , velocity standard deviation v_{rms} and number of droplets N_{drops} .

label	N^3	L (cm)	T_L (s)	Re_λ	ϵ ($m^2 s^{-3}$)	η (cm)	τ_η (s)	σ_s^0 (%)	v_{rms} (ms^{-1})	N_{drops} ($\times 10^5$)
(a)	64^3	9	2.0	40	10^{-3}	0.1	0.1	1.5×10^{-3}	4×10^{-2}	0.93
(b)	128^3	18	3.5	65	$9. \times 10^{-4}$	0.1	0.1	3.4×10^{-3}	$5. \times 10^{-2}$	8.2
(c)	256^3	38	5.5	105	10^{-3}	0.1	0.1	6.1×10^{-3}	$7. \times 10^{-2}$	71.2
(d)	512^3	70	7.6	185	1.1×10^{-3}	0.1	0.1	1.2×10^{-2}	$1. \times 10^{-1}$	320